

EXPERIMENTAL STUDY OF INSTANTANEOUS VELOCITY-PRESSURE CORRELATIONS BY PIV MEASUREMENT IN A TURBULENT PIPE FLOW WITH DRAG REDUCTION BY ADDED SURFACTANT

Takuya Yoshida

Graduate School of Science and Technology
Keio University
Hiyoshi 3-14-1, Yokohama 223-8522, Japan
y_takuya_0330@keio.jp

Shinnosuke Obi

Department of Mechanical Engineering
Keio University
Hiyoshi 3-14-1, Yokohama 223-8522, Japan
obsn@mech.keio.ac.jp

ABSTRACT

This study investigates the Reynolds stress transport process in surfactant turbulent pipe flow, aiming to elucidate how surfactants affect turbulent momentum transfer. Utilizing stereoscopic particle image velocimetry (PIV), we captured the instantaneous velocity field across the pipe's cross-section. To comprehensively analyze the Reynolds stress transport, both velocity and pressure gradient fields were essential. We derived the pressure gradient field from velocity data by numerically solving the Poisson equation. Our findings reveal a significant reduction, approximately 20%, in Reynolds shear stress attributable to the presence of surfactants. Moreover, we computed the production term and velocity-pressure gradient term from the measured velocity field. While the production term balances with the velocity-pressure gradient term for both water and surfactant flows, these terms are notably smaller for surfactant-laden flows. This suggests that the suppression of Reynolds shear stress is primarily driven by the suppression of the production term. Additionally, the velocity-pressure gradient term is also diminished to maintain equilibrium within the Reynolds stress equation, suggesting the reduction of the redistribution of energy between normal stress components which is a key mechanism of maintaining the Reynolds stress. These insights deepen our understanding of how surfactants modulate turbulent momentum transport in pipe flow.

INTRODUCTION

By adding polymers to turbulent flows, it was revealed by Toms (1949) that the flow rate within pipes can be increased significantly without increasing the pressure gradient. Furthermore, Mysels (1949) announced that surfactants have a similar effect to polymers. That is, polymers and surfactants have the effect of reducing turbulent friction, known as drag reduction.

While the effects of both are similar, surfactants, unlike polymers, have the advantage of maintaining their effectiveness even under shear stress from pumps and other sources. Surfactants induce drag reduction through micellar structures,

allowing the drag reduction effect to persist even if the micellar structure is disrupted by shear. Thus, surfactants can be utilized as drag-reducing agents even in systems equipped with pumps.

Numerous studies have been conducted on the hydrodynamic effects of surfactants, such as the suppression of turbulent eddies and Reynolds shear stress reduction, by e.g., Kawaguchi *et al.* (2002) and Hadri and Guillou (2010). In particular, the suppression of Reynolds shear stress leads to a decrease in wall friction, as indicated by the FIK identity equation proposed by Fukagata *et al.* (2002). However, there is limited research focusing on the fundamental transport processes underlying Reynolds stress generation in pipe flows. Therefore, this study aims to experimentally track the Reynolds stress transport process in turbulent flows with added surfactants.

To analyze the transport process outlined in the Reynolds stress equation, experimental evaluations of its constituent terms are essential. Given that certain terms involve pressure gradients, the pressure field is estimated from velocity field data acquired through experiments. The present study introduces a novel experimental approach to evaluate the instantaneous pressure field using velocity data obtained from cross-sectional pipe flow measurements via stereo PIV. Subsequently, the method will be presented in detail, along with validation based on DNS data.

GOVERNING EQUATION Momentum Equation

We consider a fully developed turbulent flow through a circular pipe, assuming the fluid to be incompressible. After Reynolds decomposition, the mean axial momentum equation is expressed in cylindrical coordinates as:

$$0 = -\frac{\partial P}{\partial z} + \frac{1}{r} \frac{\partial}{\partial r} r \left(\mu \frac{\partial V_z}{\partial r} - \rho v_r v_z \right), \quad (1)$$

where the z axis runs along the center line of the pipe and r is in the radial direction, originating from the center of the pipe. P denotes the mean pressure, V_z represents the mean velocity component in the z direction, and μ and ρ stand for the dynamic viscosity and density of the fluid, respectively, which we assume constant over the field. The last term within the bracket signifies the Reynolds shear stress. The symbols in upper case denote mean values, while those in lower case represent fluctuations around them. The overbar indicates variables averaged over time.

Reynolds Stress Transport Equation

The transport equation for the Reynolds stress is derived by multiplying the fluctuating velocity component with the equation for fluctuating momentum. In fully developed turbulent pipe flow, the Reynolds shear stress, denoted as τ_{12} and defined as the average of the product of the fluctuating velocities v_z and v_r , is given by e.g. Eggels (1994):

$$0 = -\overline{v_r^2} \frac{\partial V_z}{\partial r} + \frac{1}{\rho} \overline{p} \frac{\partial v_z}{\partial r} + \frac{1}{\rho} \overline{p} \frac{\partial v_r}{\partial z} - \frac{1}{r} \frac{\partial}{\partial r} \overline{r v_r^2 v_z} + \frac{v_r v_\theta^2}{r} - \frac{1}{\rho} \left(\frac{\partial \overline{v_z p}}{\partial r} + \frac{\partial \overline{v_r p}}{\partial z} \right) + \frac{1}{r} \frac{\partial}{\partial r} \overline{r v} \frac{\partial v_z v_r}{\partial r} - \overline{v} \frac{v_z v_r}{r^2} - 2\nu \left[\frac{\partial v_r}{\partial r} \frac{\partial v_z}{\partial r} + \left(\frac{1}{r} \frac{\partial v_r}{\partial \theta} - \frac{v_\theta}{r} \right) \left(\frac{1}{r} \frac{\partial v_z}{\partial \theta} \right) \right], \quad (2)$$

where ν stands for the kinematic viscosity, $\nu = \mu/\rho$. The terms on the right-hand side of Eq. (2) represent, line-by-line, the production, redistribution, diffusion by turbulent motion, molecular diffusion, and viscous dissipation of τ_{12} . Under high Reynolds number conditions, the terms associated with molecular viscosity, namely molecular diffusion and viscous dissipation, can be neglected; for the latter, local isotropy of turbulence is assumed.

After the rearrangement to the pressure-related terms, we obtain a simplified transport equation of τ_{12} in the fully developed turbulent pipe flow:

$$0 = -\overline{v_r^2} \frac{\partial V_z}{\partial r} - \frac{1}{\rho} \left(\overline{v_z \frac{\partial p}{\partial r}} + \overline{v_r \frac{\partial p}{\partial z}} \right) - \frac{1}{r} \left(\frac{\partial}{\partial r} \overline{r v_r^2 v_\theta} - \overline{v_z v_\theta^2} \right). \quad (3)$$

The second term on the right-hand side of Eq. (3) combines the pressure-strain correlation and the pressure diffusion terms from Eq. (2), conventionally termed Π_{12} . Consequently, it partially functions as a sink and partially contributes to spatial transportation, along with the third term containing the triple velocity correlation known as turbulent diffusion.

Our intention is to experimentally analyze this equation using the velocity field data acquired by measurement. The terms containing only velocity can be evaluated by appropriately interpolating the field velocity data, while those containing pressure require some approximation. We describe our approach in the next section.

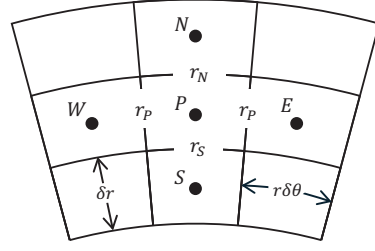


Figure 1: Control volume arrangement for the discretization of the Poisson equation of pressure.

Poisson Equation for Pressure

The pressure term in Eq. (3) can be determined by solving the Poisson equation derived from the divergence of the momentum equation. In cylindrical coordinates, the Poisson equation is expressed as:

$$\frac{1}{r} \frac{\partial}{\partial r} \left(r \frac{\partial \hat{p}}{\partial r} \right) + \frac{1}{r^2} \frac{\partial^2 \hat{p}}{\partial \theta^2} = \rho \left\{ \frac{1}{r} \frac{\partial \hat{v}_\theta^2}{\partial r} - \left(\frac{\partial \hat{v}_r}{\partial r} \right)^2 - \frac{2}{r} \frac{\partial \hat{v}_r}{\partial \theta} \frac{\partial \hat{v}_\theta}{\partial r} \right\}. \quad (4)$$

Here, the variables with $\hat{\cdot}$ represent instantaneous values. The derivative with respect to the z -direction is omitted because we have no access to it from the velocity field measurement on a single cross-section. The influence of this neglect will be discussed later in reference to the DNS data.

Equation (4) can be numerically solved under appropriate boundary conditions, e.g., Obi & Tokai (2006), provided that the information on the right-hand side is available from measurements. On the pipe wall, we assume $\partial p/\partial r = 0$, as we cannot directly measure the pressure itself. Instead, we can evaluate the pressure gradient, enabling a reliable estimation of the pressure term in Eq. (3).

We adopt here the discretized form of Eq. (4) with respect to the cylindrical control volumes shown in Fig. 1 as:

$$a_N \hat{p}_N + a_S \hat{p}_S + a_E \hat{p}_E + a_W \hat{p}_W - a_P \hat{p}_P = S_P, \quad (5)$$

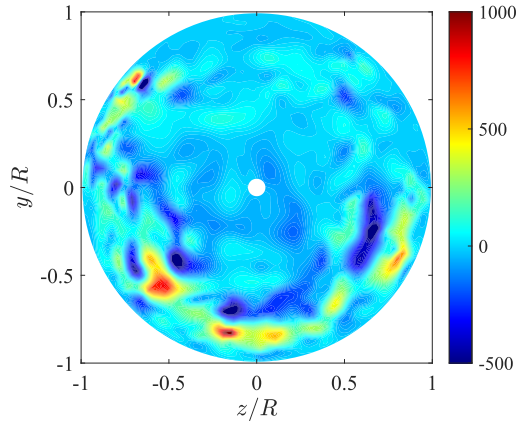
where

$$a_N = \frac{r_n \delta \theta}{\delta r} \\ a_S = \frac{r_s \delta \theta}{\delta r} \\ a_E = a_W = \frac{\delta r}{r_P \delta \theta} \\ a_P = a_N + a_S + a_E + a_W$$

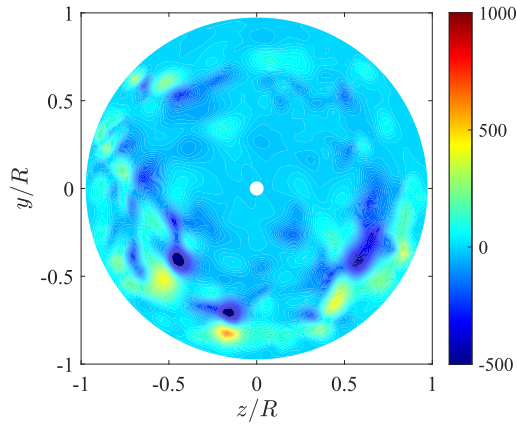
and

$$S_P = \left\{ \frac{\partial \hat{v}_\theta^2}{\partial r} - \left(\frac{\partial \hat{v}_r}{\partial r} \right)^2 + 2 \frac{\partial \hat{v}_r}{\partial \theta} \frac{\partial \hat{v}_\theta}{\partial r} \right\}_P. \quad (6)$$

Here, the velocity gradients on the right-hand-side are evaluated from algebraic operation of the velocity field data ac-



(a) Directly calculated from pressure by DNS.



(b) Obtained by solving Poisson equation based on the DNS velocity data.

Figure 2: Comparison of the instantaneous pressure gradient $\partial \hat{p} / \partial r$ in a pipe cross section. Contours are shown in arbitrary scale.

quired by a stereo PIV system introduced in the subsequent sections.

The entire cross-section of the pipe was discretized into a grid of 50×120 control volumes in the radial and circumferential directions. The size of each control volume remained uniform throughout the grid. An iterative solution approach was employed to solve Eq. (5), with the radial direction solved using the tridiagonal matrix algorithm method and then swept through the circumferential direction. The iteration process continued until the iteration-by-iteration variation of the pressure gradient at monitor points was reduced to the convergence criteria of approximately 10^{-2} . Typically, 30 iterations were conducted until convergence was achieved.

Validation of the Pressure Estimation

In this study, only the velocity field of a single cross-section is measurable, so the z -direction velocity gradient term of the Poisson equation, as shown in Eq. (4), was neglected during pressure estimation. Therefore, it is necessary to verify the validity of the pressure estimation method. For this purpose, a comparison was made with results from direct numerical simulation (DNS) by Fukagata and Kasagi (2002). From the DNS-computed instantaneous velocity field, the pressure field was estimated based on Eq. (5), and the results were compared with the pressure field obtained from DNS.

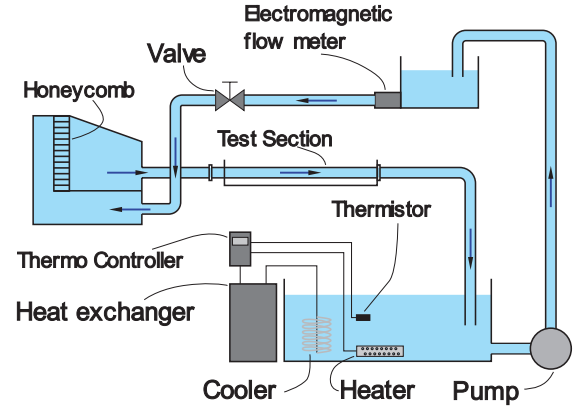


Figure 3: Circulating water tank system.

As the DNS was performed on a non-equidistant grid system of $N_r \times N_\theta = 48 \times 128$, where N_r and N_θ denote the number of grids in r - and θ -directions, respectively, the data was first interpolated on the uniform grid system by scatteredInterpolant of MATLAB™. A second-order central differencing scheme was applied to calculate the velocity gradient from these velocity data.

The distribution of instantaneous radial pressure gradient $\partial p / \partial r$ appearing in the velocity-pressure gradient term Π_{12} is compared in Fig. 2. Figure 2(a) shows the pressure gradient distribution obtained from DNS, while Figure 2(b) depicts the pressure gradient estimated by the present method from DNS velocity fields on a single cross section. From Figure 2, it can be observed that the overall distribution of the pressure field is fairly well represented by the present method. The magnitude of the pressure gradient was reduced by about 40% at most by the present method, when averaged over the circumferential direction. This difference is partly due to the neglect of the derivative terms with respect to z direction and partly due to the errors in numerical procedure such as interpolation error.

Nevertheless, we conclude that the accuracy of the pressure-related correlation terms in the subsequent discussion is sufficiently high for the purpose of comparison between water and surfactant-loaded flows.

EXPERIMENT

We conducted experiments in a closed-loop water tunnel facility as shown in Figure 3. The fluid flow was driven by the head difference between the head tank and the downstream tank, with flow rate regulation achieved through a globe valve. The Reynolds number, defined as $Re = U_b D / \nu$, was adjusted to the range of $Re = 1.1 \times 10^4$ within a few percent of accuracy. Here, U_b and D represent the bulk velocity and diameter of the circular pipe, respectively.

The test section comprised an acrylic pipe with an inner diameter of $D = 30$ mm, positioned at a distance of 1110 mm ($\approx 37D$) downstream from the entrance of the test section. According to White (2016), the entrance length was estimated about $16.4D$ for the present Reynolds number, hence the fully developed pipe flow was achieved at the location where the velocity measurements using stereo PIV were conducted on a perpendicular cross-section of the main flow. In the experiments involving surfactants, we used LSP-01M drag-reducing agent from Shunan Water Treatment Co., Ltd., adjusted to a concentration of 200 ppm. The fluid temperature was main-

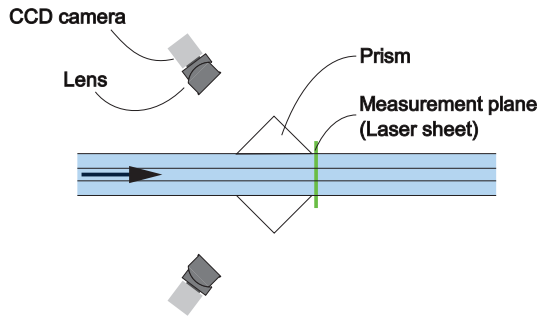


Figure 4: Setup for stereo PIV measurement.

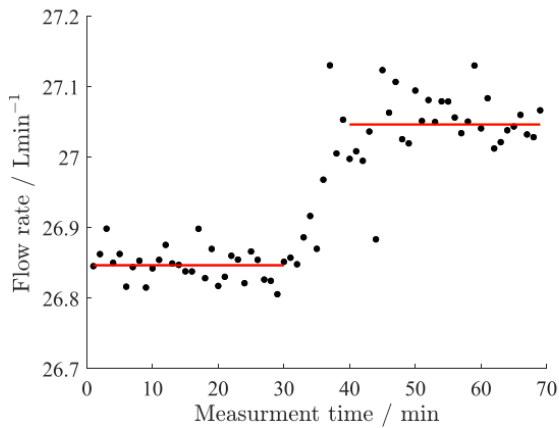


Figure 5: Variation of the flowrate as a consequence of added surfactant.

tained to be 19°C for both water and surfactant solution.

The stereo PIV system consisted of two CCD cameras (Princeton Instruments, MegaPlusII ES2020), a laser (New Wave Research, Nd:YAG dual-pulse laser, Solo-II-30), and optical lenses (PC Micro-Nikkor 85 mm f/2.8D). The arrangement of the cameras and laser sheet is shown in Figure 4. The arrangement resembles to the work of Li *et al.* (2006). The laser and cameras were synchronized by pulses, capturing paired images at a rate of 4 Hz.

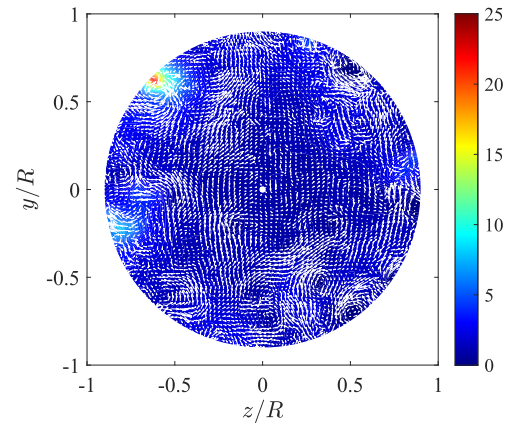
For the tracer, we used white nylon particles of 30 μm in average diameter. The cameras had 1200 \times 1600 pixels, and the interrogation area consisted of a matrix of 16 \times 16 pixels. The acquired images were processed using software developed by Suryadi *et al.* (2010), yielding velocity fields. Totally 4832 velocity vectors were acquired on the measuring plane.

We estimate the ambiguity associated with the individual velocity vector measurement to be about 5% with respect to the bulk velocity U_b .

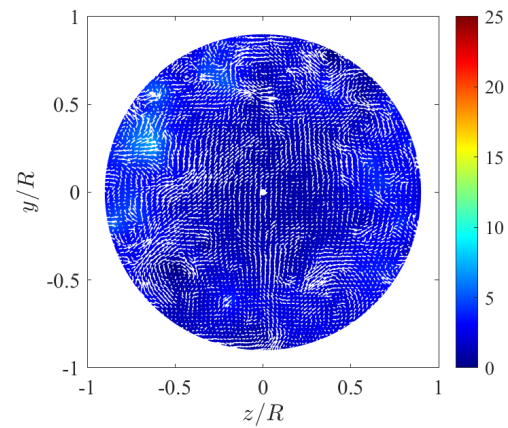
RESULTS AND DISCUSSIONS

Drag Reduction by the Surfactant

Prior to the velocity field measurement, the effect of surfactant was examined. Figure 5 demonstrates that the flow rate through the pipe was increased by adding 200 ppm surfactant. Once we had made sure that the flow rate had reached a stable state, we carried out the velocity measurements.



(a)



(b)

Figure 6: Instantaneous velocity vector on a pipe cross section and estimated pressure field. Pressure values are shown on arbitrary scale. (a) Water; (b) Surfactant solution.

Instantaneous velocity field

Figure 6 presents the measured instantaneous velocity field represented by vectors, with the estimated pressure field shown in contour plots. The velocity vectors on the r - θ plane, v_r and v_θ were smaller than the axial velocity component v_z by an order of magnitude. From Figure 6, it can be observed that the entire cross section is covered by streamwise vortex motion. Accordingly, the estimated pressure field undergoes rapid changes at positions where the velocity changes abruptly, indicating a certain degree of correlation between the velocity and pressure fields. Additionally, the maximum pressure values are observed near the wall, consistent with the instantaneous pressure field obtained from DNS in Figure 2.

By comparing Figure 6(a) and (b), we can notice that the magnitude of pressure fluctuation is diminished by adding the surfactant. The reduction of pressure fluctuation tends to alter the energy redistribution process among the individual Reynolds stress components which has been also found by a numerical study by Yu *et al.* (2004) in a turbulent channel flow. This is also an indication that the vortex motion across the cross section is suppressed and hence the momentum transfer by Reynolds shear stress.

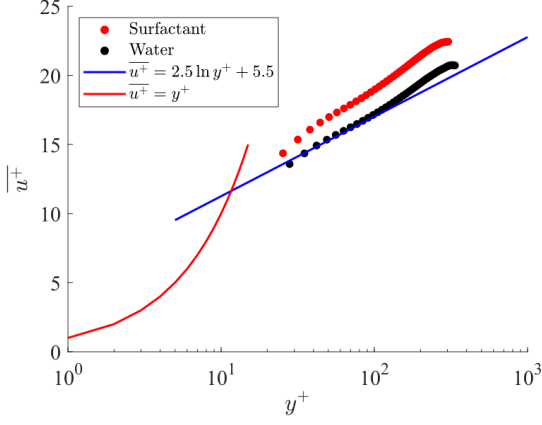


Figure 7: Comparison of mean velocity for water and surfactant of 200 ppm.

Mean velocity field

The velocity vectors acquired by the stereo PIV are defined on the Cartesian coordinate, so they are transferred to the cylindrical coordinate prior to the further process. The data were then obtained by averaging 5000 samples over time and further averaged in the circumferential direction for both water and surfactant solution.

Figure 7 compares the streamwise mean velocity profiles, with both horizontal and vertical axes normalized by the friction velocity to approximate the profiles according to the log law. The friction velocity for the water flow was evaluated according to Colebrook's formula:

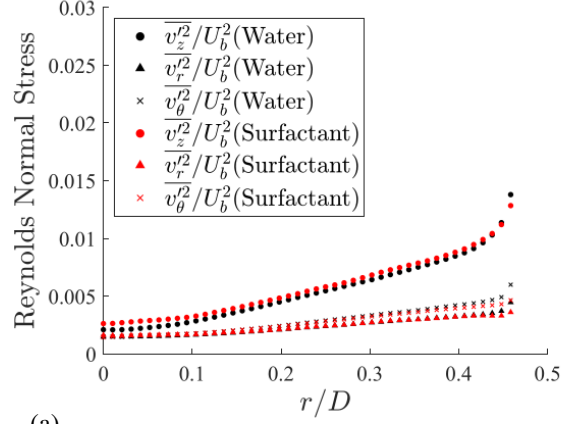
$$\frac{1}{f^{1/2}} = -2.0 \log \left(\frac{\varepsilon/d}{3.7} + \frac{2.51}{\text{Re}_d f^{1/2}} \right),$$

with the wall-roughness ε being set to zero, while for the surfactant flow we have estimated a reduction of about 10% as we observe the reduction of Reynolds shear stress of 20% as described later. It is seen that the drag reduction results in upward shift of the mean velocity profile, which is in good agreement with relevant studies summarized by Xi (2019).

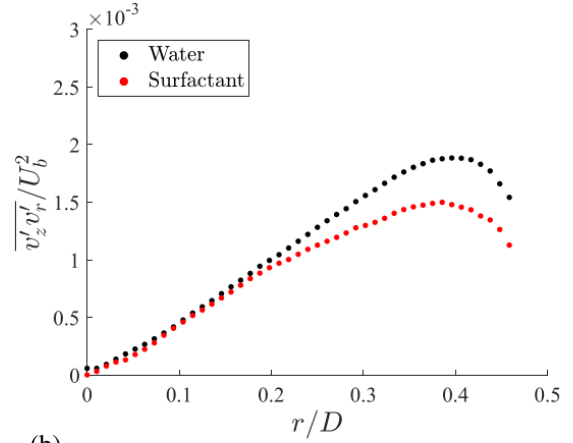
Figure 8 presents a comparison of Reynolds stress components, with (a) showing the normal stress and (b) the shear stress component. It is observed that the normal stress components are only slightly reduced by adding the surfactant, while the shear stress component exhibits a reduction of about 20% compared to water. As the shear stress profile is nearly linear close to the pipe centerline, it is again confirmed that the flow is well developed at this cross-section. The reduction in Reynolds shear stress aligns well with the observed reduction in pipe friction, indicating good accordance with drag reduction.

Budget of Transport Equation

Next, the results of calculating the production term P_{12} and the velocity-pressure gradient term Π_{12} from Eq. (3) are shown in Figure 9. According to Eq. (3), the terms P_{12} and Π_{12} are expected to balance with each other. For water, it can be confirmed that they are in close balance for the region $r \leq 0.4$. However, for $r > 0.4$, it is evident that the magnitude of P_{12} is larger than that of Π_{12} . For surfactants, it can be observed that both P_{12} and Π_{12} exhibit distributions similar to those for



(a)



(b)

Figure 8: Comparison of Reynolds stresses for water and surfactant solution, (a) Normal stresses; (b) Shear stress.

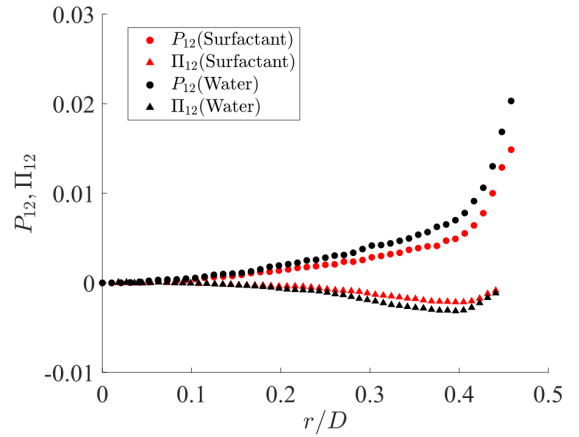


Figure 9: Budget of the transport equation for τ_{12} comparing water and surfactant of 200 ppm.

water. However, their magnitudes are smaller than those for water.

We expect that the turbulent transport terms may partly fill the difference between these terms, though, admittedly, the resolution of the measurements in the near-wall region is rather low, providing relatively large errors. Nevertheless, the pressure fluctuation in the fully turbulent region could be re-

sonably well captured, and the reduction of the Π_{12} term in surfactant flow was addressed by the present experiment.

CONCLUSION

To experimentally track the Reynolds stress transport process of surfactants flowing inside pipes, we measured the instantaneous velocity field of circular pipe cross-sections using stereo PIV. Additionally, we estimated pressure gradient distributions from the measured instantaneous velocity fields by integrating the pressure Poisson equation.

The experiments confirmed that surfactants suppressed Reynolds shear stress. Furthermore, the calculation results of the production term and the velocity-pressure gradient term revealed that the balance between these terms was maintained for both water and surfactants. However, for surfactants, both the production term and the velocity-pressure gradient term were smaller in magnitude compared to water.

These results suggest that surfactants reduce Reynolds stress (τ_{12}) by suppressing the production term (P_{12}). Furthermore, from the calculation results of the velocity-pressure gradient term, it was found that the suppression of the production term corresponded to the suppression of the velocity-pressure gradient term. In other words, it can be said that the production term was suppressed while maintaining the balance of the Reynolds stress equation.

ACKNOWLEDGEMENT

The authors are grateful to Dr. Koji Fukagata for providing the DNS data and fruitful discussion. The assistance by Dr. Takuya Kawata and Mr. Masao Kawai to conduct the initial stage of the experiment is greatly acknowledged.

REFERENCES

Eggels, J. G. M. 1994 *Direct and Large Eddy Simulation of Turbulent Flow in a Cylindrical Pipe Geometry*. Delft University Press.
Fukagata, K, Iwamoto, K & Kasagi, N 2002 Contribution

of Reynolds stress distribution to the skin friction in wall-bounded flows. *Physics of Fluids* **14** (11), L73–L76.
Fukagata, K & Kasagi, N 2002 Highly energy-conservative finite difference method for the cylindrical coordinate system. *Journal of Computational Physics* **181** (2), 478–498.
Hadri, F. & Guillou, S. 2010 Drag reduction by surfactant in closed turbulent flow. *International Journal of Engineering Science and Technology* **2**.
Kawaguchi, Y, Segawa, T, Feng, ZP & Li, PW 2002 Experimental study on drag-reducing channel flow with surfactant additives - spatial structure of turbulence investigated by PIV system. *International Journal of Heat and Fluid Flow* **23** (5), 700–709.
Li, F.-C., Kawaguchi, Y., Hishida, K. & Oshima, M. 2006 Investigation of turbulence structures in a drag-reduced turbulent channel flow with surfactant additive by stereoscopic particle image velocimetry. *Experiments in Fluids* **40** (2), 218–230.
Mysels, K. J. 1949 United states patent 2492173.
Obi, S. & Tokai, N. 2006 The pressure-velocity correlation in oscillatory turbulent flow between a pair of bluff bodies. *International Journal of Heat and Fluid Flow* **27** (5), 768–776.
Suryadi, A., Ishii, T. & Obi, S. 2010 Stereo PIV measurement of a finite, flapping rigid plate in hovering condition. *Experiments in Fluids* **49** (2), 447–460.
Toms, B. A. 1949 Some observations on the flow of linear polymer solutions through straight tubes at large Reynolds numbers. *Proceedings of the International Congress on Rheology*.
White, F. M. 2016 *Fluid Mechanics 8th Edition in SI Units*. The McGraw-Hill Education.
Xi, Li 2019 Turbulent drag reduction by polymer additives: Fundamentals and recent advances. *Physics of Fluids* **31** (12).
Yu, B., Li, F. & Kawaguchi, Y. 2004 Numerical and experimental investigation of turbulent characteristics in a drag-reducing flow with surfactant additives. *The International journal of heat and fluid flow* **25** (6), 961–974.